Acta metall. Vol. 33, No. 7, pp. 1195–1204, 1985
Printed in Great Britain. All rights reserved

0001-6160/85 $3.00 + 0.00
Copyright © 1985 Pergamon Press Ltd

THE EFFECT OF INTERDIFFUSION ON THE INTERFACIAL MICROSTRUCTURE OF Au–Pd

M. HWANG,† D. E. LAUGHLIN‡ and I. M. BERNSTEIN

Department of Metallurgical Engineering and Materials Science and The Center for the Study of Materials, Carnegie-Mellon University, Pittsburgh, PA 15213, U.S.A.

(*Received* 17 *June* 1982; *in revised form* 23 *January* 1985)

Abstract—The interfacial microstructure of {001} twist interphase interfaces in gold–palladium bicrystal thin film couples has been investigated by transmission electron microscopy. Experimental results demonstrate that the character and spacing of the interfacial dislocations change with annealing. In particular the dislocations become progressively screw dominated with increasing annealing time and/or temperature, indicating that the lattice parameters change at the interface. These values approach each other due to interdiffusion with concomitant compositional changes. The structural evolution of the interfaces due to annealing was also studied. In gold–palladium couples, evidence was found for the presence of two intermediate phases. A model for the possible stages of the structural evolution during annealing is proposed, based on detailed considerations of both microstructure and diffraction observations.

Résumé—Nous avons étudié par microscopie électronique en transmission la structure d'interfaces interphases de torsion {001} dans des couples minces bicristallins d'or–palladium. Nos résultats expérimentaux montrent que le caractère et l'espacement des dislocations interfaciales changent avec le recuit. En particulier, les dislocations deviennent progressivement majoritairement vis lorsqu'on augmente le temps et/ou la température de recuit, ce qui montre que les paramètres réticulaires changent à l'interface. Leurs valeurs s'approchent l'une de l'autre, du fait de l'interdiffusion avec changement de composition. Nous avons également étudié l'évolution structurale des interfaces due au recuit. Dans les couples or–palladium, nous avons mis en évidence la présence de deux phases intermédiaires. Nous proposons un modèle pour les étapes possibles de l'evolution structurale au cours du recuit, modèle qui repose sur la considération détaillée d'observations de microstructure et de diffraction.

Zusammenfassung—Die mikroskopische Struktur von {001}-Drill-Phasengrenzen in dünnen Filmpaaren aus Gold-Palladium-Bikristallen wurde im Durchstrahlungselektronenmikroskop untersucht. Die Beobachtungen zeigen, daß sich Charakter und Abstand der Grenzflächenversetzungen mit dem Ausheilen verändern. Insbesondere nehmen die Versetzungen mit zunehmender Ausheilzeit und/oder Temperatur immer stärkeren Schraubencharakter an. Diese Beobachtung weist auf eine Änderung des Gitterparameters an der Grenzfläche hin. Die Werte des Gitterparameters nähern sich gegenseitig durch Interdiffusion und den daraus folgenden Änderungen der chemischen Zusammensetzung an. Die Entwicklung der Grenzflächenstruktur während des Ausheilens wurde ebenfalls untersucht. In den Gold–Palladium-Paaren ergaben sich Hinweise auf zwei Zwischenphasen. Ein Modell wird für die möglichen Stufen in der Entwicklung der Grenzflächenstruktur beim Ausheilen vorgeschlagen; es folgt aus genauen Beobachtungen der mikroskopischen Struktur und aus Beugungsuntersuchungen.

INTRODUCTION

A detailed characterization of the interphase interfacial microstructure of gold–palladium prior to interdiffusion has been presented previously [1]. The twist interphase interfaces present in these bi-metallic thin film couples contain dislocation networks similar to the twist grain boundary dislocation structure reported by Balluffi and his coworkers [2–6]. In particular, the {001} twist interphase interface of gold–palladium is characterized by a dislocation network consisting of two mutually perpendicular sets of dislocations. These dislocations are of mixed edge and screw character in contrast to the pure screw character for the twist grain boundary dislocations [2–6]. The edge-character component accommodates the lattice parameter difference between the dissimilar metals and the screw character component accommodates the twist misfit.

We also established previously that the dislocation character, described by σ, the angle between the dislocation line and the respective Burgers vector, and the associated dislocation spacing, S_D, for specimens annealed for short time and/or low temperature (e.g. 400°C for 3 min) was in excellent agreement with theoretical values calculated from an accommodation model based on the lattice parameters of the pure gold and palladium [7]. However, such a bimetallic thin film couple containing an interface parallel to its surfaces is certainly not in its most stable configuration. In fact, if the two components are completely soluble, an alloy with a uniform composition throughout the whole specimen thickness should be produced after complete interdiffusion. In

†Formerly with Wang Laboratories, Inc., Lowell, MA 01851, U.S.A., now with AT and T, Bell Laboratories, North Andover, MA 01845, U.S.A.

‡On leave at the Department of Metallurgy and Science of Materials, Oxford University, Oxford, England.

Table 1. The experimental and predicted values of S_D and σ for Au–Pd annealed at different temperatures and times

T(°C)	t(min)	$\Delta\theta$(°)	$S_{D,exp}$(Å)	$S_{D,pre}$(Å)	σexp(°)	σpre(°)
400	3	4.5	31 ± 3	31	29 ± 4	31
500	50	4.5	36 ± 3	31	10 ± 4	31
550	70	4.5	35 ± 3	31	5 ± 4	31

bimetallic systems with more limited solubility, as for example, gold and palladium [8], changes upon annealing should include the possible formation of intermediate phases.

In this paper, we report our findings on the interfacial microstructure changes which occur during significant interdiffusion of gold–palladium thin film couples. The sequential steps associated with such changes can be used to devise a model for the interfacial microstructure evolution during annealing. This approach can summarize successfully much of our experimental observations in a consistent manner, although it can not yet completely predict all details of the structural evolution.

EXPERIMENTAL

The gold–palladium bicrystal thin film couples investigated in this study were prepared by the method described in a previous publication [1]. In brief, vacuum evaporated single crystal thin films of gold and palladium, with thicknesses of about 400 and 800A respectively, were placed on a TEM-grid, one on top of the other, to form a bicrystal thin film couple of controlled orientation. The as-formed gold–palladium thin film couples were placed in an Al_2O_3 boat and annealed in a tube furnace in one atmosphere of flowing purified argon gas. The annealing temperature and time were the major variables in this study. In general, the temperatures ranged from 400° to 700°C and the annealing times from 1 minute to several hours.

The annealed specimens were subsequently examined on either a JEOL 100C transmission electron microscope or a JEOL 100CX scanning transmission electron microscope equipped with an X-ray energy dispersive spectrometer to perform microchemical analyses. Both microscopes were operated at 100 kV and were equipped with a double-tilt goniometer stage, capable of a tilt of $\pm 36°$ on one axis and $\pm 60°$ on a perpendicular axis. Conventional bright-field and selected-area-diffraction techniques were utilized throughout this study, as was a technique termed $2\frac{1}{2}$D [9–11]. This latter technique is useful in helping to identify a new phase, particularly when its orientation and crystal structure are such that the reflections from it are close to the fundamental reflections of the matrix.

EXPERIMENTAL RESULTS AND DISCUSSION: CHARACTERIZATION OF THE INTERFACIAL MICROSTRUCTURE AFTER INTERDIFFUSION

As previously reported [1], the dislocation character described by σ, the angle between the dislocation line and the respective Burgers vector, and the dislocation spacing, S_D, of specimens annealed at 400°C for 3 min are in excellent agreement with predicted values [7]. However, experimental results on S_D and σ from specimens annealed at higher temperatures and/or for longer times no longer agree with these predicted values. For example, in specimens with a twist angle, $\Delta\theta$, of 4.5°, annealed at 500°C for 50 min and at 550°C for 70 min, the experimental dislocation spacing, S_D, are larger and the accompanying angles, σ, are much smaller than those predicted (see Table 1). The most likely explanation for this apparent discrepancy is that the lattice parameter difference at the interface has decreased after the extended annealing, due to interdiffusion between the bimetallic thin films.

Such interdiffusion between gold and palladium thin films will change the composition profile in the thin-film couple as well as the composition-dependent

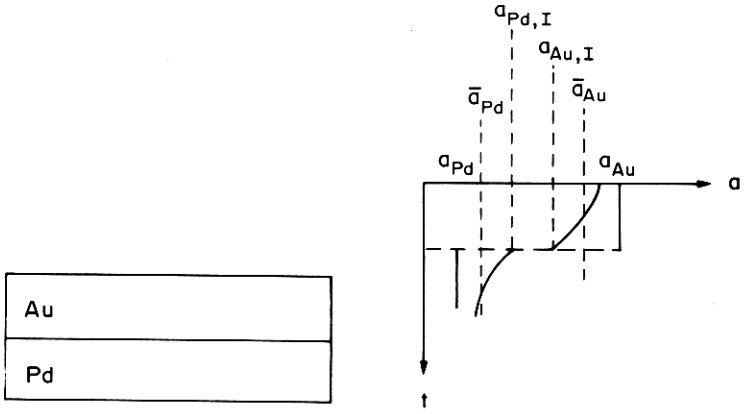

Fig. 1. A proposed lattice parameter profile in the Au–Pd specimen during annealing. The definitions of the various terms are in the text.

Table 2. The experimental values of K and K_I for Au–Pd annealed at different temperatures and times, compared to $K_0 = a_{Au}/a_{Pd} = 1.0483$

T(°C)	t(min)		K	K_I
400	3	4.5	1.046 ± 0.005	1.045 ± 0.005
500	50	4.5	1.024 ± 0.005	1.014 ± 0.005
550	70	4.5	1.010 ± 0.005	1.007 ± 0.005

lattice parameter. The proposed lattice parameter profile in the gold-palladium thin film couple during annealing is illustrated schematically in Fig. 1 where a_{Au} and a_{Pd} are the lattice parameters of pure gold and pure palladium respectively; $\bar{a}_{Au}$ and $\bar{a}_{Pd}$ are the average lattice parameters of the alloyed gold-rich and palladium-rich thin films respectively; and $a_{Au,I}$ and $a_{Pd,I}$ are the lattice parameters of the gold-rich and palladium-rich films at the interface. The average lattice parameters, $\bar{a}_{Au}$ and $\bar{a}_{Pd}$, are determined from obtained diffraction patterns using the pure gold reflection as the standard. The lattice parameters of the thin films at the interface, $a_{Au,I}$ and $a_{Pd,I}$, are calculated from experimental dependencies of S_D and σ vs $\Delta\theta$ (see Appendix). A new set of parameters, K_0, $\bar{K}$ and K_I, can thus be defined as the ratios of a_{Au}/a_{Pd}, $\bar{a}_{Au}/\bar{a}_{Pd}$ and $a_{Au,I}/a_{Pd,I}$, where K_o, the ratio of the lattice parameters of pure gold and pure palladium, is 1.0483. The experimental results for $\bar{K}$ and K_I are listed in Table 2 for specimens with a twist angle of 4.5°. From the proposed lattice parameter profile (shown in Fig. 1), the relation $1 < K_I < \bar{K} < K_0 = 1.0483$ is predicted. The experimental results are in general agreement with this relation, demonstrating that the proposed profile is certainly correct in shape, if not in absolute magnitude. The discontinuity of the lattice parameter profile at the interface at this stage of annealing is supported not only by the fact that the experimental values of K_I are not equal to unity, but also by the fact that the interfacial dislocations show edge character. Nevertheless, as interdiffusion proceeds, K_I approaches unity, the dislocation character becomes screw dominated (i.e. σ approaches zero), and the lattice parameter profile becomes continuous at the interface.

New phases in annealed gold–palladium thin film couples

Interdiffusion between thin film couples with complete mutual solubility, like gold–silver [8], will eventually produce couples with a uniform composition throughout the thickness. However, in a system with the possible formation of intermediate phases, such as gold–palladium (see Fig. 11), the situation can become considerably more complex.

Evidence for two distinct interfaces has been observed in a number of gold–palladium specimens annealed at 550° for 5 min; see Fig. 2(a). One of these interfaces has a dislocation network similar to that observed in specimens with a short time anneal at 400°C for 3 min, as presented previously (1). The dislocation spacing, S_D, of 23 Å and the angle, σ, of

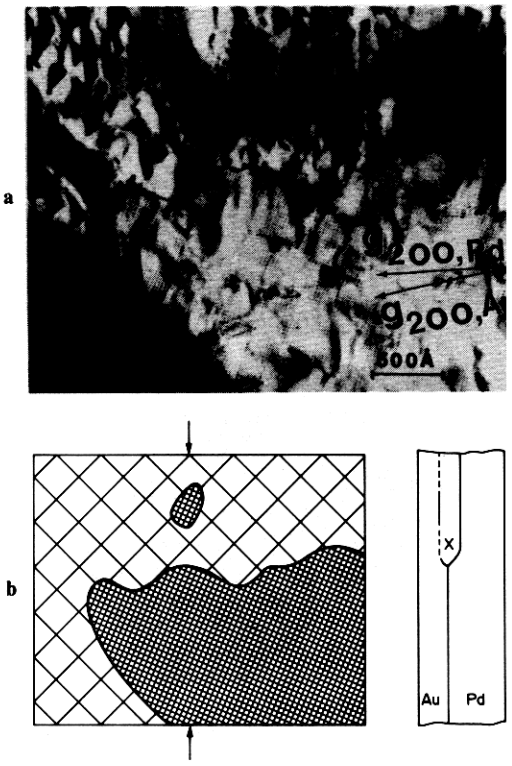

Fig. 2. (a) Two distinct interfacial dislocation networks exist. The fine dislocation network (with 23 Å spacing) shown in the lower half is the interfacial dislocation structure between gold and palladium and the new phase formed epitaxially on the palladium film. The coarse moire fringes that intercept the orthogonal coarse dislocations diagonally is also shown. The fine moire fringes in the upper half is due to the gold and palladium (or the new phase) $\mathbf{g}_{200}$ diffractional interference. The presence of fine moire fringes and the coarse dislocations indicates that a three layer structure exists in this area. (b) Schematic illustration of the dislocation structure shown in (a). A cross-sectional sketch of the specimen at the location indicated by the arrow heads is also shown to the right. The solid lines between phases represent the interfaces. The dotted line between Au and X indicates that the boundary exists; however, no interfacial structure has formed yet. This corresponds to the fine moire fringes observed in (a). Phase X is the new phase formed as the result of interdiffusion.

22° for this interface are in the range predicted for the pure gold–pure palladium twist interfacial dislocations; see the lower half of Fig. 2(a). The other interface, however, has a much larger spaced dislocation network; S_D is about 144 Å, and the dislocations are nearly pure edge in character, with respect to palladium; see the upper half of Fig. 2(a). The coarse dislocation network is probably between Pd and the new phase formed epitaxially on the palladium film. Fine spacing moire fringes were also observed in the upper half of Fig. 2(a). This is due to $\mathbf{g}_{(200)}$ diffractional interference of gold and palladium (or possibly the new phase). The presence of fine moire fringes in the absence of the fine dislocation structure indicates that the gold film and the new phase is not yet welded together at this area. A schematic illustration of the dislocation structure of

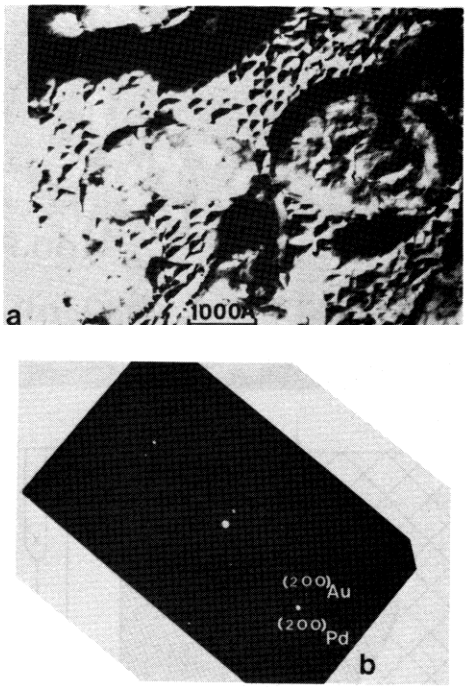

Fig. 3. (a) An Au–Pd interface with two distinct dislocation networks (annealed at 550°C for 5 min). (b) The electron diffraction pattern of (a) with the proper rotation.

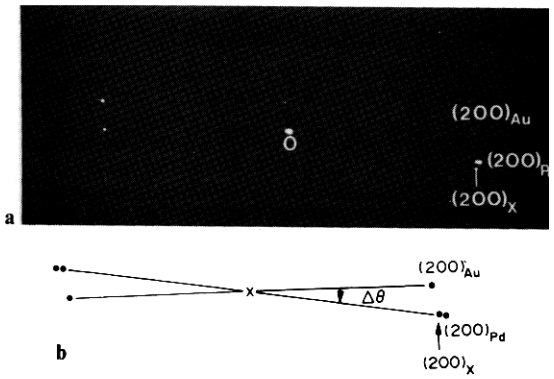

Fig. 4. (a) The $\mathbf{g} = (200)$ two-beam electron diffraction pattern of an Au–Pd specimen with two distinct interfaces (annealed at 550°C for 5 min). An extra reflection, designated as $(200)_x$, near the (200) Pd reflection with the same orientation as palladium and of magnitude $|\mathbf{g}\,(200)_x|$ is smaller than $|\mathbf{g}\,(200)_{Pd}|$ but larger than $|\mathbf{g}\,(200)_{Au}|$. (b) Schematic illustration of (a).

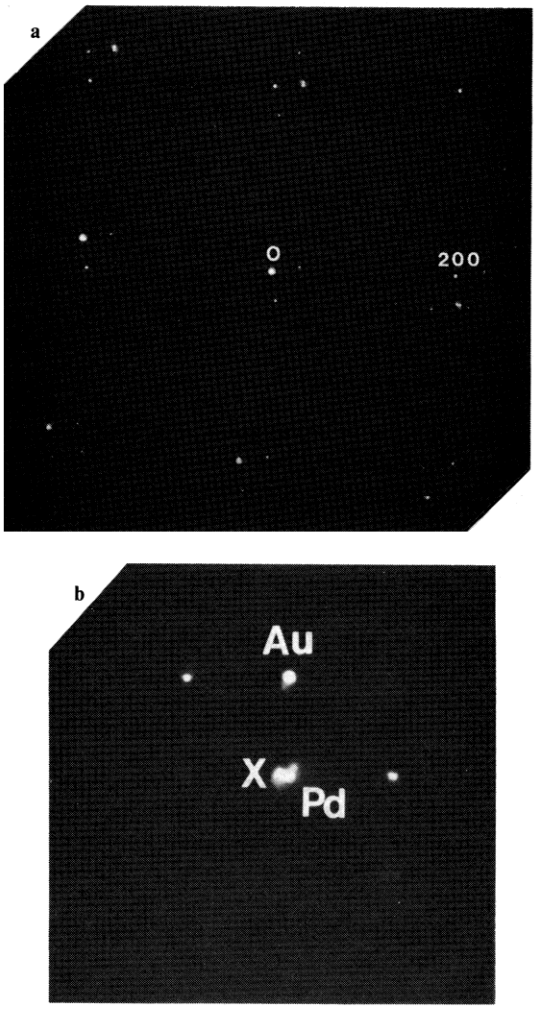

Fig. 5. (a) The electron diffraction pattern of an Au–Pd specimen with two distinct interfaces (annealed at 550°C for 5 min). Double diffraction reffections, in addition to the extra reflection described in Fig. 4, can be observed. (b) Detailed configuration of one of the (200) reflections shows the characteristic three-layer double diffraction shown schematically in Fig. 7 (below).

Fig. 2(a) is shown in Fig. 2(b). A cross-sectional sketch of the specimen at the location indicated by the allow heads is also shown to the right; the top-on view shows the coarse and the fine dislocation networks. The cross-sectional view shows that there are three phases (namely gold-rich, the new phase, and palladium-rich phase) present in the upper half and only two phases (gold-rich and palladium-rich phases) exist in the lower half of the sample observed in Fig. 2(a). The solid lines between phases represent the interfaces. The dotted line indicates the boundary between gold and the new phase; however, no interfacial structure has yet formed in this area.

The $2\frac{1}{2}$D technique was applied to help differentiate between these two interfaces. A pair of bright-field images of the area shown in Fig. 3(a), one slightly overfocused and the other slightly underfocused, was taken. The resultant stereo pair image showed the two interfaces to be separated, implying that these two interfaces are the boundaries between different phases [9,11]. Thus, at least three phases are present in the thin film couple at this stage.

The diffraction pattern for this specimen also shows extra reflections near the palladium reflections. These have the same orientation as palladium, and a lattice parameter larger than palladium but smaller than gold; see Fig. 4. This fine diffraction pattern structure was studied in some detail. In addition to the strong extra reflections near the fundamental palladium reflections, a group of weak diffraction spots associated with each of the gold and palladium spots was also observed (Fig. 5). The geometry of

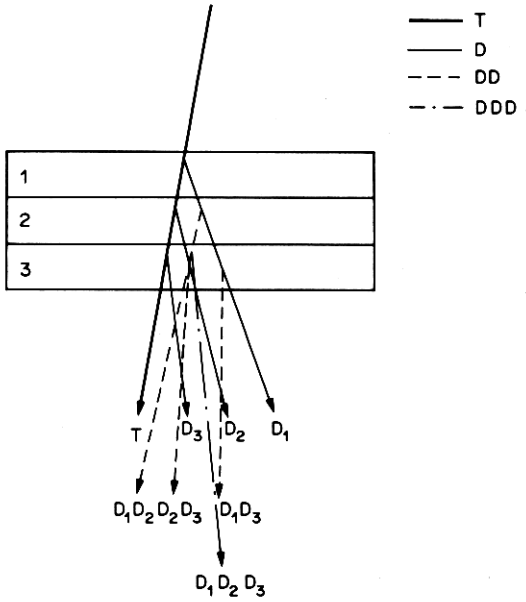

Fig. 6. A three-layer schematic film to illustrate possible multiple electron diffraction interactions: T is the transmitted beam; D is the diffracted beam; DD is the double diffracted beam; and DDD is the triple diffracted beam.

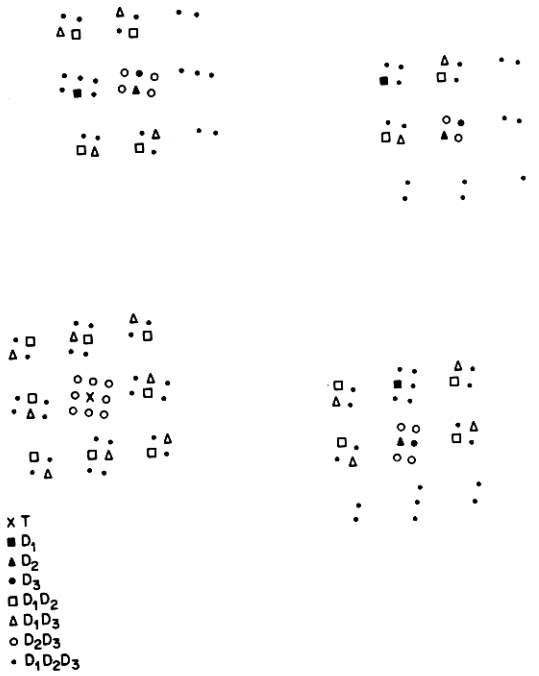

Fig. 7. The complex diffraction pattern resulting from double (or multiple) diffraction of a three-layer film shown in Fig. 6, with the assumptions described in the text.

such a group of spots was found to be consistent with the expected double or multiple diffraction pattern of a three-layer film arranged as shown in Fig. 6. The transmitted beam, T, can be diffracted by layer 1, 2 or 3; the diffracted beams are represented as D_1, D_2 and D_3 respectively. Also, the D_1 beam can be diffracted by layer 2 or 3; these diffracted beams are represented as D_1D_2 and D_1D_3 respectively. The D_2 beam and the D_1D_2 beam can be diffracted by layer 3; these diffracted beams are represented as D_2D_3 and $D_1D_2D_3$ respectively. To generate a resultant diffraction pattern we assume the following: (i) these three layers are all f.c.c. single crystals with a common [001] axis perpendicular to the film surface; (ii) the lattice parameter of layer 1, a_1, is greater than that of layer 2, a_2, and both a_1 and a_2 are greater than that of layer 3, a_3; and (iii), $\langle 001\rangle_2$ of layer 2 is parallel to $\langle 001\rangle_3$ of layer 3, but it has a slight twist misorientation with respect to $\langle 001\rangle_1$ of layer 1. Following this line of reasoning, a part of the schematic complex diffraction pattern can be generated as shown in Fig. 7, which is consistent with the observed diffraction pattern shown in Fig.5.

A simpler diffraction pattern for a two-layer film is helpful in understanding the geometrical feature of the three-layer film diffraction pattern. A schematic of the diffraction pattern, without layer 2, is shown in Fig. 8 and is characterised by a group of points clustered around each fundamental reflection. The group of points form a square pattern with a spacing equal to the shortest vector between the two equivalent fundamental reflections from the two layers. In the three-layer diffraction pattern, this periodic character appears around not only each fundamental reflection group, but also around each of the fundamental reflections themselves. The experimental evidence found here for such a diffraction pattern is shown in Figure 5(a), for characteristic two-layered film diffraction. With careful examination, the additional characteristic diffraction spots also can be seen around each of the fundamental spots; see, e.g. Fig. 5(b).

Identification of the new phases

Both the bright-field images and the nature of the diffraction patterns suggest that a third phase forms between the gold–palladium films after extended

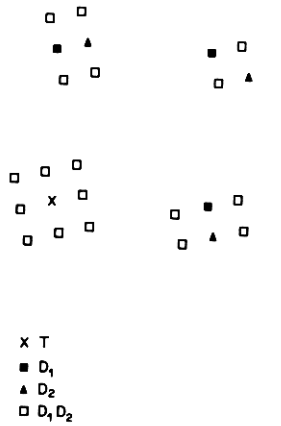

Fig. 8. The simpler diffraction pattern results from double diffraction of a two-layer film similar to the three-layer film shown in Fig. 6, but now without layer 2. Note the characteristic square arrangement of the diffraction spots around each fundamental reflection.

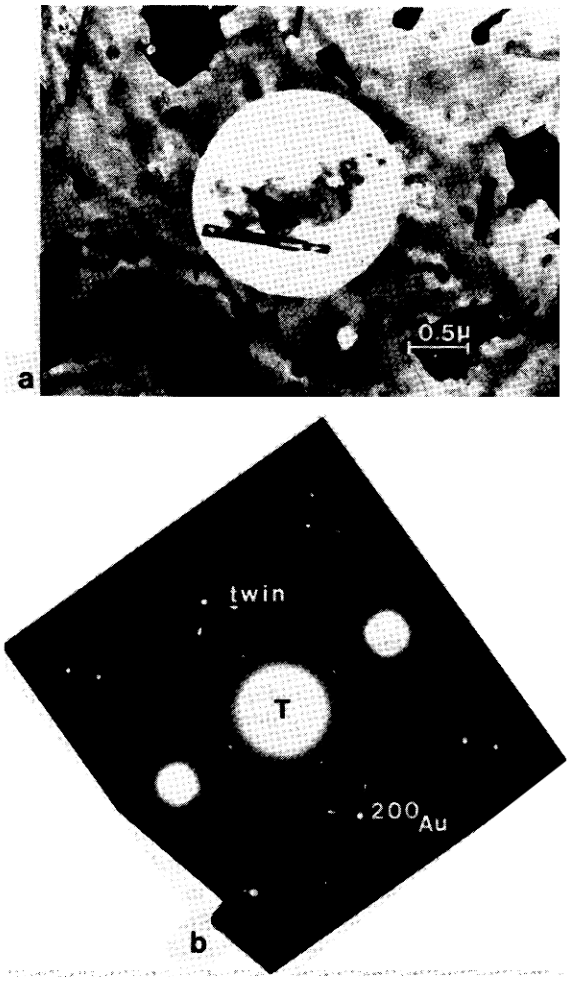

Fig. 9. (a) A bright-field image of an Au–Pd specimen after extended interdiffusion occurs (annealed at 550°C for 4 h). The brighter circled area is the area from which the SAD pattern of part (b) was taken. (b) The SAD pattern showing the {100} and {110} type superlattice reflections expected from the ordered $L1_2$ structure. Four extra reflections near each fundamental reflection are due to microtwin reflections. This pattern is the same orientation as the original [001] pattern of gold.

annealing. The most likely stoichiometry of this new phase is the ordered intermediate phase $AuPd_3$ with the structure of Ll_2 [8]. For such a structure, ordered reflections are expected to appear at the {100} and {110} positions. Efforts to find these ordered reflections in this specimen were not successful. This is most likely because of the small volume fraction of the ordered phase. Another reason could be a low degree of order in the $AuPd_3$ phase [13, 16].

However, superlattice reflections of the {100} and {110} types with respect to the fundamental gold reflections were observed (see Fig. 9) in another gold–palladium specimen which was prepared on gold rather than tungsten grids and subsequently annealed. In this case, micro-chemical analysis showed that the average composition integrated over the whole specimen thickness is about three-fourths gold to one fourth palladium. This specimen was likely to be completely alloyed throughout the whole thickness, since no interfaces were found in the area examined. The structural and chemical analyses results suggest that this ordered phase formed is probably the gold-rich $AuPd_3$ phase, also exhibiting the Ll_2 structure [13, 16].

A proposed model for the interfacial microstructure evolution during annealing

Our experimental observations have shown that the developing interfacial microstructures of gold–palladium thin film couples, where the thickness of the gold and palladium films are 400 Å and 800 Å respectively, can incorporate the formation of either or both Au_3Pd and $AuPd_3$ intermediate phases. The interdiffusion coefficient of Au–Pd thin films [18] is about 2.9×10^{-14} cm^2/s at 400°C for 2–3 min, conditions for which the interfacial microstructure of nearly pure gold and pure palladium was observed. Since the estimated diffusion distance $2(Dt)^{1/2}$ is about 370 to 450 Å, no significant interdiffusion took place at this stage. The formation of the intermediate phase, $AuPd_3$, was observed in specimens annealed at 550° for 5 min, where the estimated diffusion distance

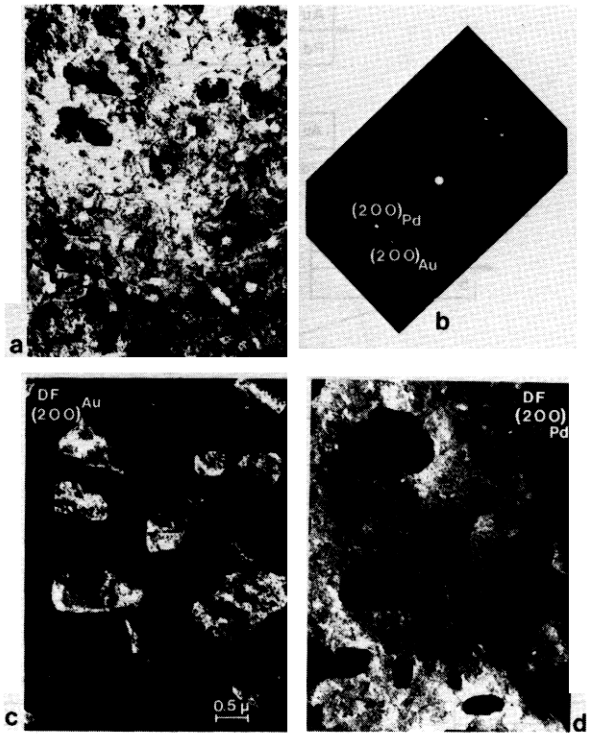

Fig. 10. (a) A bright-field image of a recrystallized Au–Pd specimen (annealed at 500°C for 3 hr. (b) The electron diffraction pattern of (a) properly rotated. (c) The dark-field image of $(200)_{Au}$. (d) The dark-field image of $(200)_{Pd}$. The recrystallized grains adopt either the starting orientation of gold or palladium.

is now 1500 Å. From interdiffusion distance considerations it is probable that diffusion extends far enough so that $AuPd_3$ phase may now form, although further annealing is required for homogenization to proceed. Experimental observation on specimens annealed at 550° for 70 min (corresponding to 5600 Å in the diffusion distance) showed that the compositions of two films are approaching each other (see Tables 1 and 2). As homogenization proceeds, the interface parallel to the specimen surface can thus be eliminated and the specimen then recrystallized by a process similar to that reported for the gold twist grain boundary case [17]. In support, a specimen annealed at 500°C for 3 h (corresponding to the diffusion distance of 6900 Å) showed the recrystallized structure (see Fig. 10). The recrystallized grains, having the composition of the overall alloy, usually take on the orientation of either the original gold or palladium thin film.

An idealized model for the evolution of the interfacial microstructure can be proposed in order to characterize the experimental observations. This model was constructed based on the equilibrium phase diagram as well as diffusion considerations. Phases 1 to 5 presented in this model are defined as follows: phase 1 is the gold-rich solid solution with an f.c.c. structure; phase 2 is the ordered Au_3Pd with an Ll_2 structure; phase 3 is an f.c.c. alloy phase with a composition that varies between approximately 25% Pd and 75% Pd; phase 4 is the ordered phase $AuPd_3$ with an Ll_2 structure; and phase 5 is the palladium-rich solid solution with an f.c.c. structure (see Fig. 11). The sequences of the presence of these phases in the annealed gold–palladium thin film couple may be summarized as follows (see Fig. 12).

Step I Pure gold and pure palladium thin films exist prior to any annealing. The bright-field image shows only moire fringe contrast. Experimental observation for a similar situation of the gold–silver thin film couple was shown in Fig. 8 of the previous publication [1].

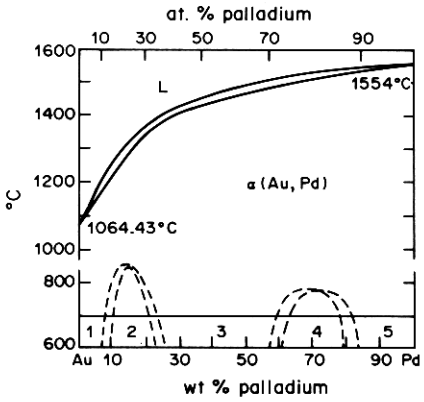

Fig. 11. Phase diagram of Au–Pd. Phases 1 to 5 are indicated to represent the possible alloy phases of different composition or crystal structures.

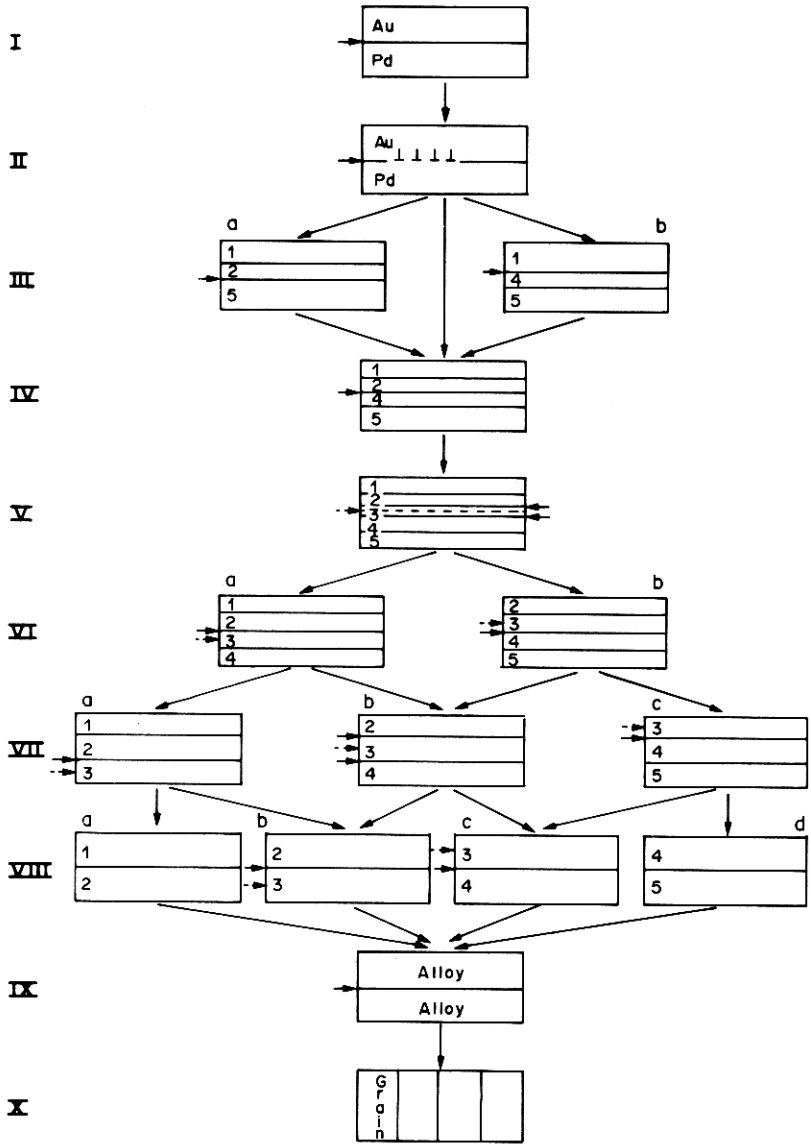

Fig. 12. The idealized model for the sequence of the possible structural evolution in Au–Pd thin film couples. The arrow heads (within the specimen) indicate the possible positions of the twist interfaces.

Step II Interfacial dislocations with the predicted mixed edge-screw character form prior to any significant interdiffusion. Experimental observation was shown in Fig. 4 of the previous publication [1].

Step III Either phase 2 (Au_3Pd), or phase 4 ($AuPd_3$), may form first between phase 1 and 5 as interdiffusion proceeds to the composition of either of these two phases at the interface. Phase 2 or phase 4 grow epitaxially on phase 1 or phase 5, respectively. The presence of phase 2 and or 4 depends on several factors, such as the relative diffusion rates of gold into palladium and palladium into gold, the composition of the starting gold–palladium couple, the temperature, and the kinetics of the formation of phase 2 and 4. If phase 2 forms epitaxially on phase 1, the twist interface remains between phase 2 and 5. In the other case, the twist interface remains between phases 1 and 4. The latter case was experimentally observed in this study (see Figs 2 and 3).

Step IV Depending on the composition profile during interdiffusion, phase 4 may form on phase 5 if phase 2 has formed in Step III: or alternatively, phase 2 may form on phase 1 after phase 4 has formed on phase 5. The twist interface now is between phases 2 and 4. This configuration may appear immediately after Step II, depending on the kinetics of the formation of phase 2 or 4.

Step V Similarly, phase 3 may form epitaxially on phase 2 or 4 or on both. The twist inter-

face will be between phases 3 and 4 or 2 and 3 or within phase 3, respectively.

Step VI The outer layers start to disappear as the composition profile of the inner phase reaches the surfaces. Phase 1 or 5 are the first phases likely to anneal out.

Step VII The same process as Step VI occurs; the three-layer specimens, with either phase 1, 2 and 3, or 2, 3 and 4, or 3, 4, and 5 remaining.

Step VIII One more layer is annealed out, leaving the two-layer specimen of phase 1 and 2, or 2 and 3, or 3 and 4, or 4 and 5.

Step IX The composition may be homogenized at this stage. The twist interphase interface becomes a twist grain boundary. Experimental evidence of this trend is indicated in Tables 1 and 2.

Step X The same processes observed in gold–gold twist grain boundary may now be expected [17]. A recrystallized specimen will take the place of the original thin film couple. Experimental evidence is shown in Fig. 10.

4. SUMMARY AND CONCLUSIONS

Characterization of the interfaces in gold–palladium thin film couples has shown that the microstructure is dependent on the annealing treatment or equivalently on the extent of the interdiffusion between gold palladium thin films. Experimental results on the dislocation structure of specimens annealed at 400°C for 3 min are in excellent agreement with the predicted values reported in our previous publication [1].

Extended annealing at higher temperatures changes the character of the interfacial dislocation structure due to lattice parameter changes at the interface. A lattice parameter profile has been proposed (Fig. 1) to explain the experimental results. The interfacial microstructure of gold-palladium thin film couples upon annealing is complicated by the possible formation of intermediate phases. Evidence for two intermediate phases, corresponding to the ordered phases of Au_3Pd and $AuPd_3$ has been obtained in some annealed gold–palladium thin film couples. The mechanism and sequence of the formation of these new phases in such thin film couples were not established definitely owing to their complex nature. However, a model which includes all possible sequences was constructed, based on the equilibrium phase diagram which is consistent with the experimental observations. This model considers phase formation from the thermodynamic and diffusional point of view, and assumes that the starting composition of the thin film couples is such that it is possible to have three, four or five layers appear at the same time. In real systems, the kinetics and mechanisms of the formation of the new phases as well as the strain energy may influence the process and therefore change the sequence. However, since Steps I, II, III, IX, and X have been experimentally observed in the present investigation, we have confidence in the reasonableness of this description. Nevertheless, the model is intended solely to summarize the experimental observations in a consistent manner and is not intended to show unequivocally how each step of the structural evolution is completed. To do so would require a much more extensive characterization including compositional studies.

Acknowledgements—The authors would like to thank Dr G. Shiflet and Mr G. Scarr for valuable discussions on the $2\frac{1}{2}$D technique. We would also like to thank Mr R. Miller for the excellent line drawings. Financial support from the National Science Foundation through Carnegie-Mellon University's Center for the Study of Materials under Grants No. DMR76-81561 and No. DMR78-24699 is also gratefully acknowledged.

REFERENCES

1. M. Hwang, D. E. Laughlin and I. M. Bernstein, *Acta metall.* **28,** 621 (1980).
2. T. Schober and R. W. Balluffi, *Phil Mag.* **20,** 511 (1969).
3. T. Schober and R. W. Bauluffi. *Phil Mag.* **21,** 109 (1970).
4. T. Schober, *Phil Mag.* **22,** 1063 (1970).
5. R. W. Balluffi, G. R. Woolhouse and Y. Komem, *Nature and Behavior of Grain Boundaries* (edited by H. Hu), Report of A.I.M.E. Symp., Detroit (1971).
6. R. W. Balluffi, Y. Komem and T. Schober, *Surf. Sci.* **21,** 68 (1972).
7. W. A. Jesser and D. Kuhlmann-Wilsdorf, *Physica Status solidi* **31,** 533 (1967).
8. *Metals Handbook*, Vol. 8, 8th edn. Am. Soc. Metals, Metals Park OH (1961).
9. W. L. Bell, *J. appl. Phys.* **47,** 1676 (1976).
10. P. Rao, *Phil. Mag.* **32,** 755 (1975).
11. R. Sinclair, G. M. Michal and T. Yamashita, *Metall. Trans.* **12A,** 1503 (1981).
12. M. Hwang, Ph.D. thesis, Carnegie-Mellon Univ., Pittsburgh, PA (1981).
13. W. D. Copeland and M. E. Nicholson, *Acta metall.* **12,** 321 (1964).
14. A. Nagasawa, Y. Matsuo and J. Kakinoki, *J. Phys. Soc. Japan* **20,** 1881 (1965).
15. Y. Matsuo, A. Nagasawa and J. Kakinoki, *J. Phys. Soc. Japan* **21,** 2633 (1966).
16. Y. Kawasaki, S. Ino and S. Ogawa, *J. Phys. Soc. Japan* **30,** 1758 (1971).
17. R. M. Allen and P. J. Goodhew, *Acta metall.* **25,** 1095 (1977).
18. S. S. Lau and R. C. Sun, *Thin Solid Films* **10,** 273 (1972).

APPENDIX

A formulation for K_1

The parameter K_1 is defined as the ratio of $a_{Au,1}$ and $a_{Pd,1}$, the lattice parameters of gold-rich and palladium-rich phases at the interface (see Fig. 1).

From the equation for the angle σ [7]

$$\sigma = \frac{\pi}{2} - \frac{\Delta\theta}{2} - \tan^{-1}\left[\frac{b_1 \sin(\Delta\theta)}{b_2 - b_1\cos(\Delta\theta)}\right].$$

If σ and $\Delta\theta$ are known, the ratio of b_2/b_1 can be obtained as follows.

First, define a new parameter α as

$$\alpha = \frac{\pi}{2} - \frac{\Delta\theta}{2} - \sigma \qquad \text{(A1)}$$

$$\text{then, } \tan\alpha = \tan\left[\tan^{-1}\frac{b_1\sin(\Delta\theta)}{b_2 - b_1\cos(\Delta\theta)}\right]. \quad \text{(A2)}$$

Simplifying equation (A2) we obtain

$$\tan\alpha = \frac{b_1\sin(\Delta\theta)}{b_2 - b_1\cos(\Delta\theta)}. \quad \text{(A3)}$$

From the definition of K_1

$$K_1 = \frac{a_{\text{Au,I}}}{a_{\text{Pd,I}}} = \frac{b_{\text{Au,I}}}{b_{\text{Pd,I}}} = \frac{b_2}{b_1}$$

where b is the Burgers vector and $b_2 = b_{\text{Au,I}} = \dfrac{a_{\text{Au,I}}}{\sqrt{2}}$ is greater than $b_1 = b_{\text{Pd,I}} = \dfrac{a_{\text{Pd,I}}}{\sqrt{2}}$.

From equation (A3) we can then derive an expression for K_1:

$$K_1 = \frac{b_2}{b_2} = \frac{\sin(\Delta\theta)}{\tan\alpha} + \cos(\Delta\theta). \quad \text{(A4)}$$